



BENDING MOMENT DISTRIBUTION ESTIMATION OF ACTUAL STEEL BUILDING STRUCTURE BY MICRO STRAIN MEASUREMENT

J. Iyama⁽¹⁾, K. Araki⁽²⁾

⁽¹⁾ Associate Professor, Graduate School of Engineering, The University of Tokyo, iyama@arch1.t.u-tokyo.ac.jp

⁽²⁾ Structural Engineer, ITEC Corporation, arakik@itec-c.co.jp

Abstract

In recent years, structural health monitoring of building structures has attracted a great deal of attention, and many monitoring systems for buildings have become commercially available. However, many of them measure the acceleration response to estimate the overall behavior of the building, such as natural period, attenuation, and inter story drift, and cannot directly measure the stress state or damage state of individual structural members.

An alternative and better measurement index to determine the state of individual structural members may be strain. It seems easy to measure strain by strain gauges, however, there are almost no examples of measuring strain in actual steel building structures. The reasons for the fact may be that the strain that occurs in the structural frame on a daily basis is extremely small and difficult to measure, and the long term durability of strain gauges is low. In addition, local strains are likely to be affected by the measurement position and the surrounding environment and it may be difficult to interpret the measured value to more understandable indexes. As a result, the data analysis method and the utilization method of such measured strain have not been established.

With the use of a highly accurate semiconductor gauge that has recently appeared, it is possible to capture extremely small strain amplitudes under microtremor. In this paper, as a fundamental study to establish of strain-based structural health monitoring technology, a micro strain measurement of an actual building was performed using a semiconductor strain gauge and analyzed.

The target structure is a 3-story steel moment frame building structure. In addition to installing three accelerometers, semiconductor strain gauges were affixed to 8 cross sections to measure the axial force and bending moment at sections of beams and columns. The data was collected over a period of 8 months, including more than 100 small earthquake motions. From the measured acceleration and strains, the ratio of bending moment at beam and/or column sections to the displacement at the top of the building, which is referred to as "local stiffness" in this paper, is calculated. This value is a physical index representing the stiffness of the structural elements near the measured location, and can be easily predicted by simple static frame analysis. The measured value is compared to the analysis value and the difference and the time change is discussed.

From the analysis of the measured data, it was shown that the measured local stiffness of beams was comparable to the analysis result, but that of columns was larger than the analysis value. This result means that non-structural members other than the beams and columns may exhibit a certain degree of restoring force, and the measured local stiffness may be affected strongly by such elements not considered as structural element at the stage of structural design. Conversely, it is possible to estimate the behavior of non-structural components from the measured local stiffness. In this measurement, both the measured predominant frequency and the local stiffness of beams and columns showed amplitude dependency, but the trend of the change of local stiffness of the beams and that of the columns are opposite. This means that the main cause of the amplitude dependency of predominant frequency is not owing the behavior of the beams and the columns, but owing to other reasons such as non-structural components and/or change of mass effect.

Through these observations, this paper showed that the strain measurement can directly grasp the dynamic behavior of structural members as well as that of non-structural members, although, in order to know more detailed behavior of non-structural members more dense measurement of strain should be necessary.

Keywords: Structural health monitoring; Steel moment frame structure; Strain measurement



1. Introduction

In recent years, structural health monitoring of building structures has attracted a great deal of attention, and many monitoring systems for buildings have become commercially available. However, many of them measure the acceleration response to estimate the overall behavior of the building, such as natural period, attenuation, and inter story drift, and cannot directly measure the stress state or damage state of individual structural members.

An alternative and better measurement index to determine the state of individual structural members may be strain. It seems easy to measure strain by strain gauges, however, there are almost no examples of measuring strain in actual steel building structures. The reasons for the fact may be that the strain that occurs in the structural frame on a daily basis is extremely small and difficult to measure, the long term durability of strain gauges is low, and the data acquisition system of dynamic strain is expensive. In addition, local strains are likely to be affected by the measurement position and the surrounding environment and it may be difficult to interpret the measured value to more understandable indexes. As a result, the data analysis method and the utilization method of such measured strain have not been established.

With the use of a highly accurate semiconductor gauge that has recently appeared, it is possible to capture extremely small strain amplitudes under microtremor. And also due to advances in IT and IoT technology, the cost of measuring device is being reduced and the feasibility of strain measurement of actual building structure is increasing.

The authors have installed accelerometer and high-precision strain gauges in a building of steel moment frame, and have measured many earthquake responses from the establishment of the building. Some of the analysis of the data have been reported in a paper[1], but in this paper more detailed analysis of the time history record is presented.

2. Measurement method

2.1 Target structure

The target structure is a 3-story steel moment frame building structure built in Fukushima Prefecture. This structure is constructed using web-clamp type beam-to-column rigid joint[2]. Fig. 1(a) to (d) shows the floor plan of the second floor, the X2 axis structure as the measurement plane, the floor slab detail and the details of the outer walls. Table 1 shows the cross-section list. Some beam-to-column joints are pin joint where only the beam web is connected to column with high strength bolts. The column base is an exposed-type column base that has undergone performance evaluation by the designated performance evaluation organization. As shown in Fig 1(c), the deck composite slab has a concrete thickness of 80mm on the deck, and the distance between the centroids of the steel beam and the concrete slab is 409mm.

2.2 Measurement

A semiconductor strain gauge was attached to the column beam surrounded by the dashed line shown in Fig. 1 (a) and (b). Fig. 2 shows the details of the measurement position. In order to measure axial force and bending moment, a total of four semiconductor strain gauges (manufactured by Kyowa Electric Instruments Co., Ltd., KSN-2-120-E4-11) are installed on the back of the H-shaped steel flange of each beam cross section for the four cross sections of the beam and the four cross sections of the column. The measured beams and columns are marked with LB(Left beam), RB(Right beam), UC(Upper column), LC(Lower column) as shown in the figure, and will be distinguished using these symbols.

In addition, accelerometers (manufactured by Kyowa Electric Instruments, ASQ-2D) are installed at three locations on the first floor(1F), second floor(2F), and the roof(RF). The strain gauges and accelerometers are

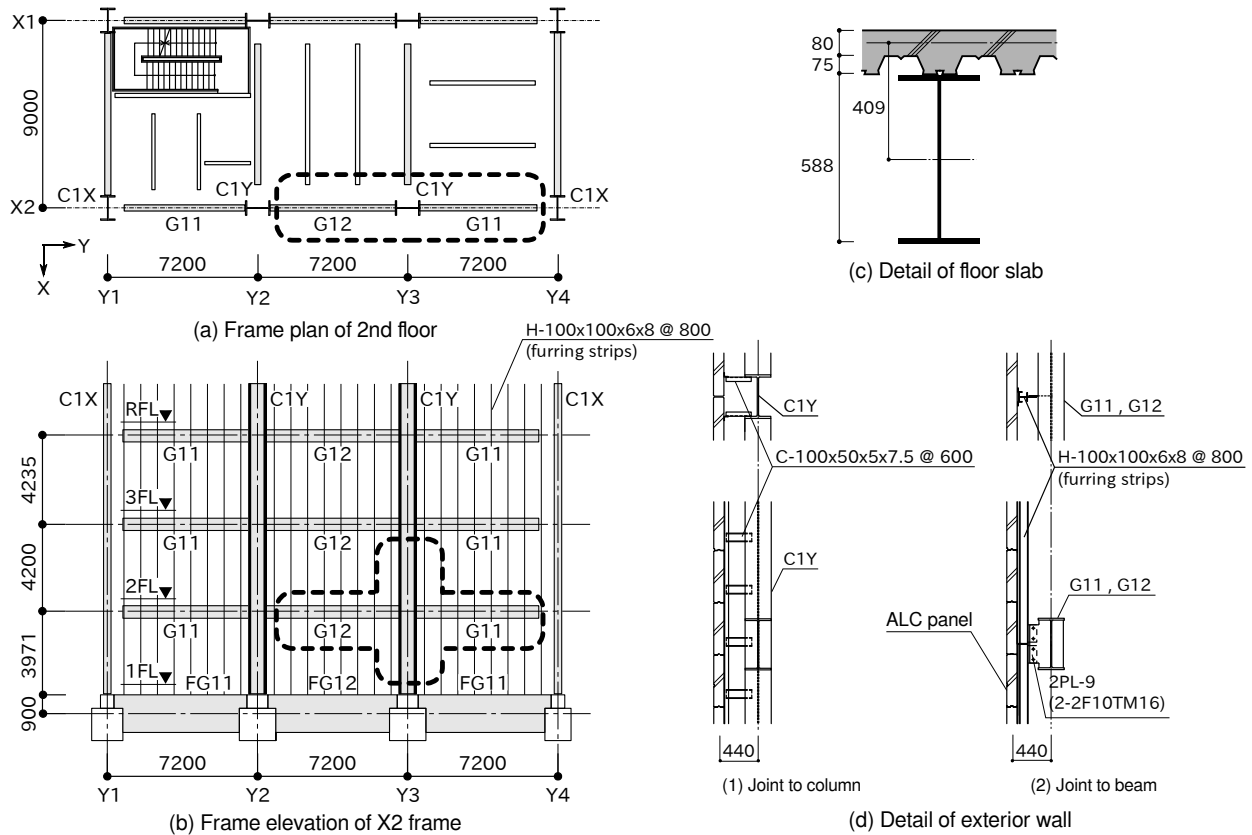


Fig. 1 – Structural frame of the target building[1]

Table 1 – Section list[1]

Section name	Section size		Z* [mm ³]
C1X, C1Y	H-shape steel	SH-500x300x16x25	43360
G11, G12	H-shape steel	H-588x300x12x20	41610
FG11	Reinforced concrete	1800x600	--

connected to a data logger (manufactured by Kyowa Electric Instruments, NTB-500A), All of which are synchronized, including strain measurement, and are measured at a sampling frequency of 100Hz.

A total of 215 small earthquakes recorded between 2018/12/14 and 2019/10/23 were analyzed. The largest earthquake experienced during this time was an M6.4 earthquake with an epicenter off Fukushima Prefecture at around 19:23 on August 4, 2019). The maximum seismic intensity reported by the Japan Meteorological Agency around the site was 4, and the maximum acceleration measured by the accelerometer installed on 1F was 102 gal.

2.3 Structural characteristics of buildings calculated on structural design

In the structural design a 3D frame analysis was performed by the commercial structural calculation software SuperBuild SS-3. The beam is treated as a composite beam, and the effect of the floor slab is taken into account by multiplying the average of the stiffness increase rates of positive and negative bending by the automatic calculation function implemented in the software. In the column base, an exposed type column base that has been evaluated by a designated performance evaluation organization is used, and was modeled as a rotational spring having a rotational stiffness described in the catalog in the structural calculation. As the measurement system is installed in a y-direction frame is measured, so only the results of the y-direction frame is shown.

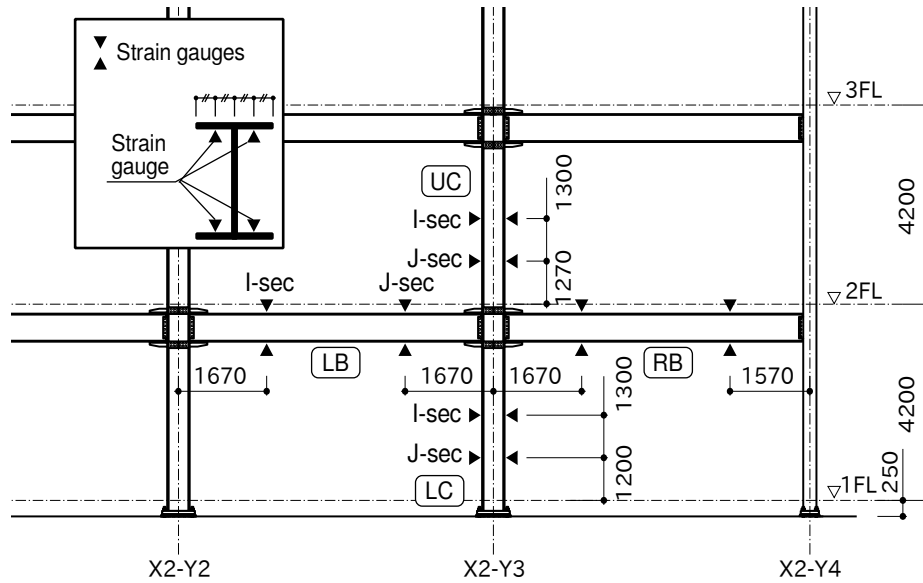


Fig. 2 – Location of strain gauges[1]

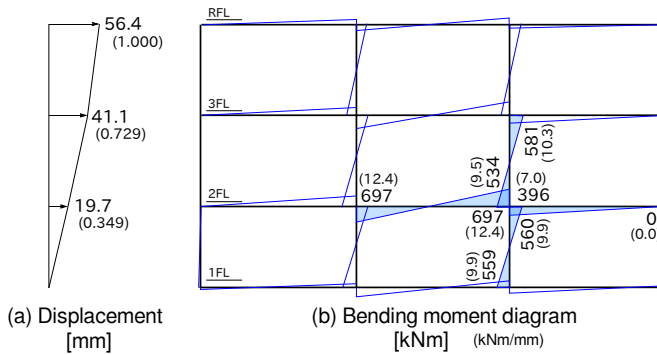


Fig. 3 – Structural calculation result of X2 frame under horizontal seismic load[1]

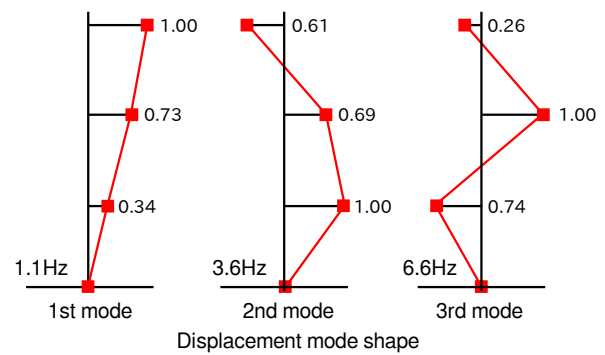


Fig. 4 – Eigenvalue analysis result[1]

Fig. 3 shows the horizontal displacement distribution and bending moment distribution under the seismic load obtained by structural analysis at the time of design. The numerical values shown in the horizontal displacement chart on the left are the horizontal displacements at each floor, and the values enclosed in parentheses are values normalized by the horizontal displacement (56.4 mm) at the roof floor (RF). On the other hand, the value shown in the right figure is the value of the bending moment in the measurement target range (unit: kNm), and the value enclosed in parentheses is the value divided by the horizontal displacement on the RF (unit : [kNm / mm]) . Since this value has the physical meaning of the bending moment of each member when unit deformation is applied to the building, it is called local bending stiffness in this paper, and is used as an index indicating the behavior of the structural member.

Fig. 4 shows the natural frequency and natural mode shape obtained in the Y-axis direction. The eigenmode shape is a shape normalized by the maximum displacement in the stories. The primary natural frequency is 1.1Hz, and the mode shape at this time almost matches the deformation shape when the seismic load shown in Fig. 3 is statically loaded.



3. Measurement result

3.1 Recorded time history and the frequency characteristics

In this section, focusing on the strongest earthquake measured around 2019-08-04T19:23+0900, time history and the frequency characteristics are shown and discussed.

3.1.1 Acceleration

Figure 5 shows an example of the relative acceleration time history in the Y direction and the Fourier amplitude spectrum measured on RF and 2F. Note that Fig. 5(b) shows the raw result of Fourier transform, $\hat{a}(f)$, without any smoothing process. The Fourier transform of acceleration, $\hat{a}(f)$, is defined in this paper as follows:

$$\hat{a}(f) = \frac{1}{L} \int_0^L a(t) e^{-2i\pi f t} dt \quad (1)$$

Here, $a(t)$ is the floor response relative acceleration at the time, and L is the duration of the target acceleration recording. Since this definition is divided by the duration L , it has a dimension of acceleration.

From Fig. 5 (b) the predominant frequencies can be read as 1.96Hz, and the peak acceleration amplitude are 0.053 [m/s²]. Fig. 5 (c) shows the difference between the phases at RF and 2F. Around the predominant frequencies, the phase difference is almost zero, which means the peak frequency captures the natural frequency of the system. In this paper, since the smoothing is not performed when selecting the predominant frequency, the selected predominant frequency may be different from the true natural frequency. However, for the calculation of the local stiffness value, it is more important that the phase of the target section force and that of the reference displacement are the same. Therefore, this paper does not focus on whether or not the selected dominant frequency is a true value but the emphasis is on whether the phases are the same.

3.1.2 Mode shape

Fig. 6 shows the vibration mode shape read from the spectrum in Fig. 5. The value of the horizontal axis of the measurement result is calculated as the ratio of the relative acceleration amplitude of the 2nd floor and the R floor at the peak frequency of the relative acceleration response of the RF, which is the same as the displacement amplitude ratio. The figure also includes the displacement distribution obtained by the eigenvalue analysis and static analysis described above. Since it is not measured on the 3rd floor, only the values on the 2nd floor can be compared, but it can be seen that the values on the 2nd floor roughly match. It is shown that, although the frequency is different, the vibration mode shape is almost the same as the calculated one.

3.1.3 Bending moment and axial force in beam

In this section, the bending moment and axial force calculated from the strain measurement is presented. The axial force and bending moment in the steel beams are calculated by the following equations from measured strains.

$$N_s(t) = EA \frac{\varepsilon_i(t) + \varepsilon_b(t)}{2}, \quad M_s(t) = EZ^* \frac{\varepsilon_i(t) - \varepsilon_b(t)}{2} \quad (2)$$

where $\varepsilon_b(t)$ and $\varepsilon_i(t)$ are average values of strain measured on the lower flange and the upper flange at the time t , respectively. E is the Young's modulus, A is the cross-sectional area, and Z^* is the section modulus, calculated by dividing the inertia moment of the section by the inner distance between flanges, since the strain gauges are pasted on the back of flanges. The axial force is indicated as positive when it is in tension, and the bending moment is indicated as positive when the upper flange is in tension.

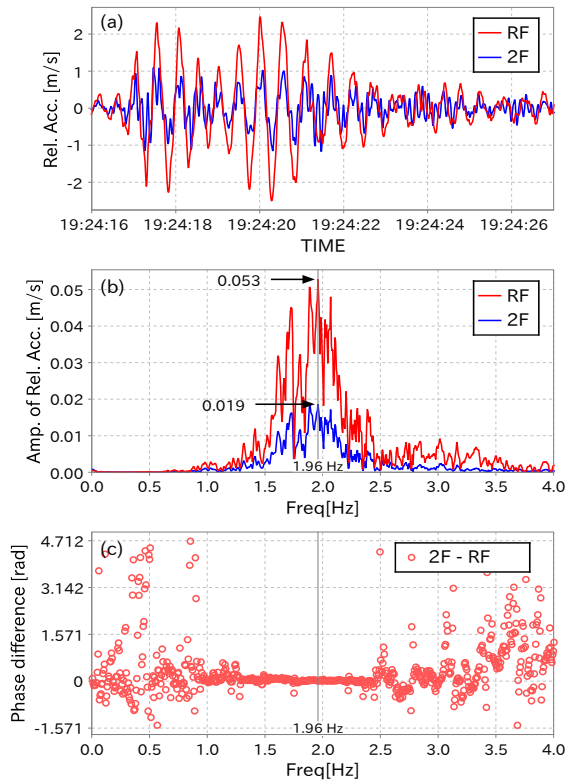


Fig. 5 – Relative acceleration recorded on the RF earthquake occurred at 2019-08-04T19:23+0900

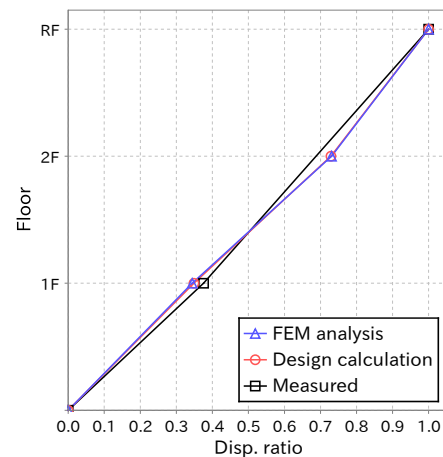


Fig. 6 – Mode shape

Fig.7 (a) shows the recorded data of the bending moment. "MI" and "MJ" represents the bending moment at I- and J-section of the right beam, respectively, calculated by Eq. (2). In the figure, the top, middle, and bottom graph shows the time history, the Fourier amplitude spectrum, and the phase difference, respectively. In the bottom figure, the vertical axis shows the phase difference of MI or MJ to that of the relative acceleration measured at RF. The phase of MI is opposite to that of MJ, which means that the beam have received the double curvature bending, and it is also opposite to that of the acceleration at RF, which means that the I-section undergoes positive bending moment when the structure deforms toward X-axis positive direction.

Fig.7 (b) shows the recorded data of the axial force. "NI" and "NJ" represents the axial force at I-section and J-section of the right beam, respectively, calculated by Eq. (2). The shape of the spectrum in Fig.7 (b) is almost the same as shown in Fig.7 (a) and the ratio of MI/MJ is almost the same as the ratio of NI/NJ. The phase of NI is opposite of MI, which means the axial force is in tension when the bending moment is the bottom flange in tension. The peak values of NI and NJ are different, which indicates that the axial force amplitudes at I- and J sections are different.

The stress distributions at the I- and J- section of LB at the predominant frequency of 1.96 Hz are illustrated in Fig. 8, which is calculated from the values shown in Fig. 7(a) based on Bernoulli-Euler theory. The axial force value with parentheses (984N and 279N) is the axial force of the floor slab estimated using the effective width of slab calculated from the design formula in current Japanese design code. For both sections, the axial force of steel beam (2451N and 400N) is much larger than the estimated axial force of concrete slab. Although it is difficult to determine the reason, it may be because the design formula may underestimate the slab's effect.

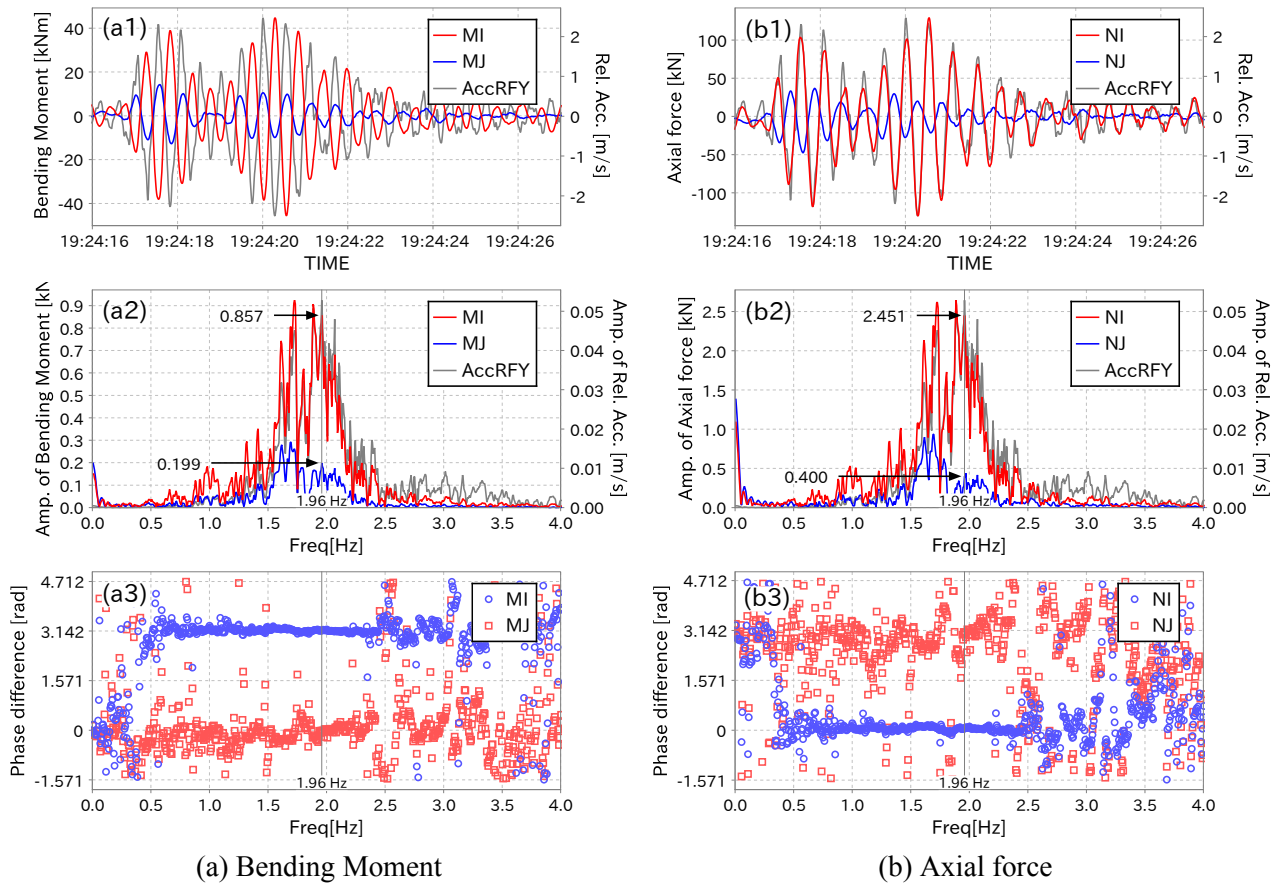


Fig. 7 – Time history and frequency characteristics of section force of RB (right beam)

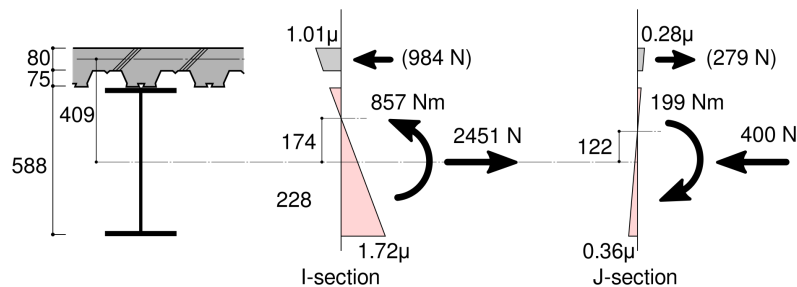


Fig. 8 – Estimated strain amplitude distribution at I- and J-section of LB at predominant frequency

In this paper, the axial force is considered mainly caused by the effect of the composite beam, and in the later calculation the bending moment of the beams is calculated by the following equation including the effect of the axial force of the concrete slab.

$$M = M_s + 409 [\text{mm}] \times N_s \quad (3)$$

3.2 Local stiffness

3.2.1 Definition of local stiffness

In Section 3.1.1, the acceleration amplitude was obtained from the response acceleration record on the R floor. In Sections 3.1.3, the axial force amplitude and bending moment amplitude in the measurement cross section were obtained. Using these, the local stiffness can be obtained by dividing the stress amplitude (axial



force amplitude or bending moment amplitude) by the displacement amplitude. Specifically, the local bending stiffness is calculated by the following equation.

$$K_i = \frac{\hat{M}_i(f_{\text{peak}})}{\hat{d}_r(f_{\text{peak}})} \quad (4)$$

where f_{peak} is the frequency, \hat{M}_i is the bending moment amplitude in a section i , and \hat{d}_r is the Fourier transform of the displacement at RF defined as follows.

$$\hat{d}_r(f) = \frac{\hat{a}_r(f)}{4\pi^2 f^2} \quad (5)$$

where $\hat{a}_r(f)$ is the Fourier transform at frequency f of $a_r(t)$.

3.2.2 Local stiffness distribution

Equation (4) was a formula for calculating the local bending stiffness only in a certain section, and can be calculated only for the section where strain is measured. However, if the bending moment distribution can be assumed as linear over the entire length of the member, the local bending stiffness is also linear over the entire length of the member. Therefore, the local bending stiffness can be calculated over the entire length of the member by linear interpolation and extrapolation. Fig. 9 shows the local stiffness distribution calculated as explained above. The values shown in the figure represents the local stiffness at the beam and column ends estimated by extrapolation from the measured section data the location of which is indicated by two transversal lines in the diagram. In the calculation of the local bending stiffness of the beam, the bending moment of beams were calculated by the above equation (3) is used. On the other hand, the broken line in Fig. 9 shows the local bending stiffness distribution obtained from the structural calculation previously shown in Fig. 4.

Since the local bending stiffness is proportional to the bending moment value, the sum of the local bending stiffness of the column and the sum of the local bending stiffness of the beam at the beam-column joint should theoretically match. However, the sum of the measured values of the column is about 1.6 times that of the beam. Although the cause cannot be determined solely from the current measurement results, one hypothesis may be that there is some unidentified members that bear stress in parallel to the beam. Fig. 10 illustrates this hypothesis as a very simple example. In this measurement, the strain gauge was attached only to the two sections of the column and the beam, respectively, and only the stress (axial force and bending moment) at this section could be measured. For this reason, in this paper, the stress at the beam-to-column joint is estimated by extrapolating the stress of the two cross sections linearly. However, assuming that there was some unidentified element that can bear stress in parallel with the beam as shown in Fig. 10, the stress would be transferred to the column but not captured by the this measurement. In this building, as described in Section 2.1 and Fig. 1(c), ALC panels are attached outside of the beams via vertical furring strips of H-section steel (H-100x100x6x8) at 800 mm intervals. It is conceivable that these fairly rigid furring strips and ALC panels can bear and transfer some stress to the columns.

3.3 Amplitude dependency

3.3.1 Amplitude dependency of predominant frequency and mode shape

Fig. 11 shows the relationship between the response dominant frequency and the displacement amplitude for the 209 small earthquakes measured. Five records out of 215 were excluded because the difference of the phases of displacements on 2F and RF are larger than 0.05 rad, where the vibration of the selected peak frequency is not considered of the 1st mode.

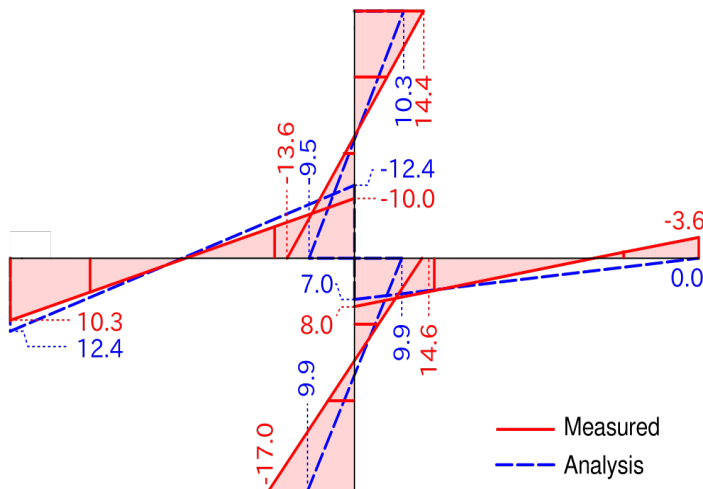


Fig. 9 – Local stiffness distribution measured during an earthquake around 2019-08-04T19:23:11+0900 [kNm/mm]

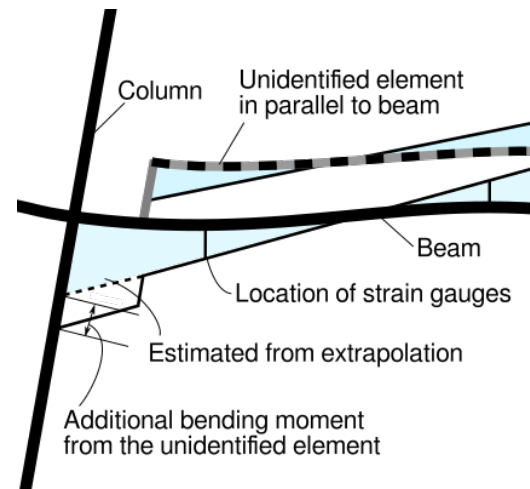


Fig. 10 – Presumed cause of stress transition by unidentified non-structural element

The displacement amplitude shown on the horizontal axis is the pseudo displacement amplitude obtained by Eq. (5). In addition, the solid line in a figure has shown the regression line. In the figure, it is represented by a curve because the horizontal axis is a logarithmic axis. In the figure, “CHG” indicates the amount of change in the start and end values of the displayed regression line, “%CHG” determines the ratio of the amount of change to the start value, and “R2” indicates the coefficient of determination (or the square of the correlation coefficient).

A tendency for the dominant frequency to decrease as the displacement amplitude increases is observed. In the range where the displacement amplitude is small, it is about 2.6 Hz, but it decreases to about 2.0 Hz as the displacement amplitude increases. The coefficient of determination shown in the figure is about 0.27, indicating that there is a certain degree of correlation. The rate of change is about -33%, and if the mass is constant and the calculation is simply made as the square root, the stiffness has dropped to about half.

Fig. 12 shows the ratio of the displacement amplitude at the second floor to the displacement amplitude at the RF to see the amplitude dependence of the mode shape. Although there is a slight downward trend, many earthquakes show stable values in the vicinity of 0.37 to 0.38, indicating that they vibrate in the primary mode shape obtained by analysis.

3.3.2 Amplitude dependency of local stiffness

Figure 13 shows the relationship between the response displacement amplitude at the R floor and the calculated local bending stiffness at the beam-column joint for all measured seismic responses. The meanings of the solid line, “CHG”, “% CHG”, and “R2” are the same as in Figs. 11 and 12.

As the displacement amplitude increases, the local bending stiffness of the beam tends to increase and the local bending stiffness of the column tends to decrease. From the regression line shown in Fig. 13, the ratio of the sum of the local bending stiffness of the column to the sum of the local bending stiffness of the beam decreases to about 2.1 times when the amplitude is small, and to about 1.4 times when the amplitude is large. This indicates that the difference between the local bending stiffness of the beam and the local bending stiffness of the column becomes smaller as the displacement amplitude increases.

However, the total amount of changes in the local stiffness of beam and column are not the same. Reading from Fig. 13, the total amount of increase in the local bending stiffness of the beam (indicated as CHG in the figure) is 4.04, whereas the total amount of decrease in the local bending stiffness of the column is 4.79. This

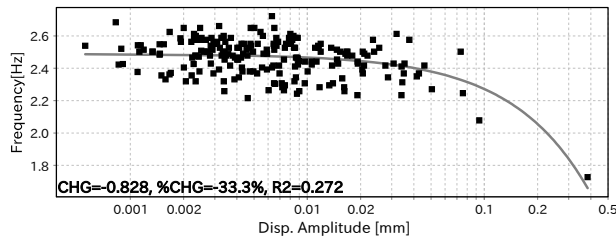


Fig. 11 – Relation between frequency and displacement amplitude

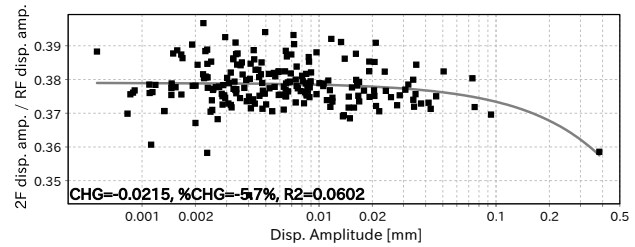


Fig. 12 – Relation between mode shape and displacement amplitude.

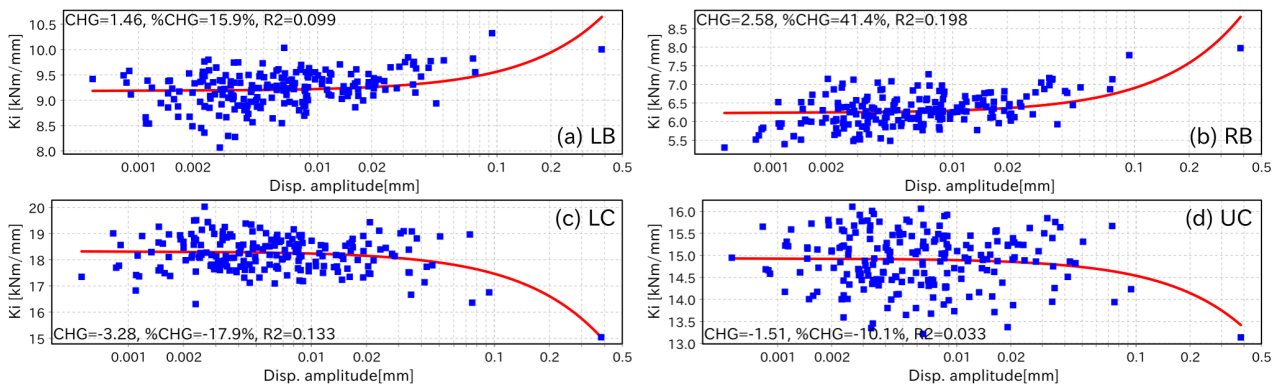


Fig. 13 – Amplitude dependency of K_i values on displacement amplitude

means that the difference between local stiffness in beam and column cannot be completely explained simply by assuming some unidentified members parallel to beam.

The average rate of decrease in the local bending stiffness of the columns is about -14%, and the change of the predominant frequency could be estimated as -7% if it could be calculated simply by a square root of stiffness change. This change is considerably smaller than the local stiffness change that is simply estimated from the change in the dominant frequency described in section 3.4 above. This means that the cause of the predominant frequency was not only the change in the local bending stiffness of the column. The reason may be, for example, the effective mass of non-structural members and equipment that contributes to building vibration may change depending on the amplitude, but the cause cannot be mentioned within the scope of this measurement, and more detailed measurements are needed.

3.4 Long-term trend

3.4.1 Long-term trend of predominant frequency and mode shape

In the previous sections, the relationship between displacement amplitude and values such as the dominant frequency and local bending stiffness has been shown, but the measurement has been over half a year and includes the effects of changes over time. In this section, the change over time of each characteristic will be examined.

The long-term change of the response dominant frequency obtained in Section 3.4 over the entire measurement period is shown in Fig. 14. Although the variation is not small, the regression line determination shows a downward trend with a coefficient of determination of about 0.4.

The long-term change of the mode shape (e.g., the ratio between displacement amplitude of 2F and RF) is shown in Fig. 15. The coefficient of determination (R^2) is very small and little long-term trend can be observed. From this result, it can be determined that the mode shape has hardly changed.



3.4.2 Long-term trend of local stiffness

Fig. 16 shows the long-term changes in the local bending stiffness of the beam and column at the beam-column joint. The coefficient of determination for the beams are less than 0.1, which means there is no clear correlation between the time and the local stiffness of the beams. However, graphs for the columns show a clear downward trend in the regression lines. The reduction ratio of the local stiffness of the columns is about 10% and the coefficient of determination is more than 0.5, showing a clear correlation.

Assuming that the stiffness of the column is reduced by 10%, this change may have caused a decrease of the predominant frequency by about 5%. This estimated value is smaller than the observed value of 10% in Fig. 14. This result shows that the column stiffness change may be one of the cause of the predominant frequency change but not the only one and there may be other causes this measurement could not capture.

4. Conclusion

In many cases, structural monitoring of actual buildings estimates the natural frequency, damping, maximum interstory deformation angle, etc. by measuring the response acceleration. However, it is not sufficient as an index that directly indicates the state or damage state. Strain can be a more direct measurement physical quantity. By performing strain measurement, it is possible to clarify the stress transmission mechanism, verify structural calculations, quantitatively evaluate structural performance degradation due to deterioration or damage, and identify damaged parts. In this paper, in order to contribute to the establishment of such a technology, dynamic strain measurement of an actual building was performed, and the stress distribution, amplitude dependence, and long-term change of the beam-column members were examined based on the results.

The measurement target building was a 3-story steel frame building. High-precision strain gauges were attached to columns and beams connected to one beam-column joint and dynamic response data were collected under 215 small earthquakes. The maximum seismic intensity reported by the Japan Meteorological Agency around the construction site during the measurement was 4.

In this paper, the value of the bending moment amplitude calculated from the strain records divided by the displacement amplitude on the roof floor was used as an index. This value indicates the member stress when the building undergoes a unit horizontal displacement, and has a physical meaning as the stiffness of the member. In this paper, this value is called "local bending stiffness."

The overall distribution of the local bending stiffness of beam and columns measured by strain gauges agreed with that estimated by a static frame analysis. However, the sums of the local bending stiffness in the beam and the column were not the same, which should be theoretically the same considering the equilibrium of the bending moment at the beam-to-column joint. This fact implies the existence of unidentified elements that can bear any force which is probably parallel to the beams. In this building, the beam is provided with a relatively strong ALC panel on the outer wall via the vertical rim, which can be considered as one of such unidentified element that bear some stress and transfer it to the columns.

In the recorded data, the amplitude dependency and log-term change were observed in the predominant frequency as well as the bending local stiffness of columns and beams. In the long-term investigation, the predominant frequency showed a clear downward trend, but the beam bending moment did not show a downward trend. From these observations, these changes may not be owing to the performance change of beams and columns, but may be owing to non-structural components like ALC panels or vertical rims.

In this paper, by measuring strain in addition to measuring acceleration response, it was shown that it is possible to separate and understand the change of structural member behavior and the non-structural member behavior, even from a very small seismic response record. As mentioned in the introduction, with regard to strain measurement in actual buildings, there are still many problems that need to be solved, such as the durability and the high cost of installing strain gauges and wiring. However, the strain measurement can

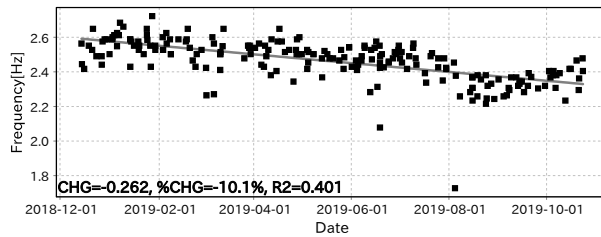


Fig. 14 – Long term trend of frequency

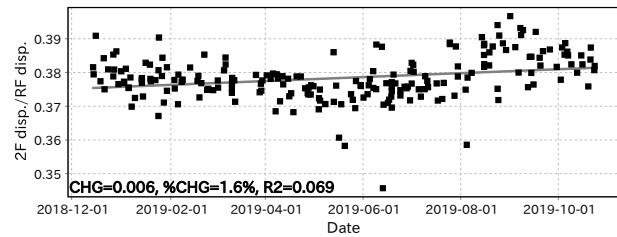
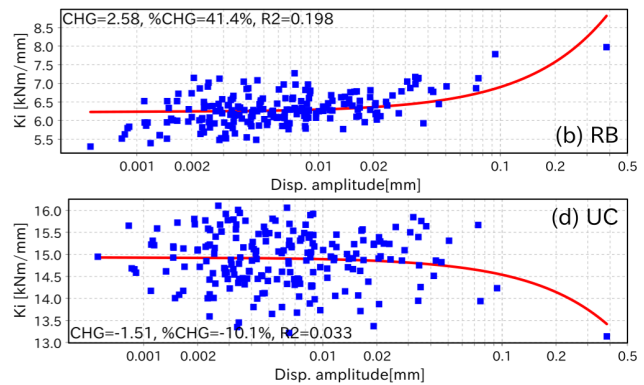
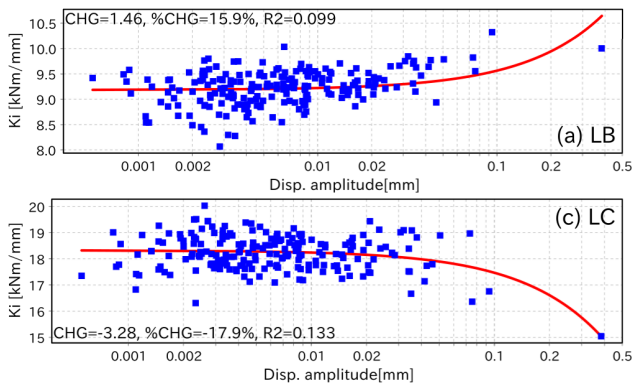


Fig. 15 – Long term trend of mode shape

Fig. 16 – Long-term trend of K_i values

provide extremely much information on the behavior and performance of the structural members as compared with the acceleration measurement alone, and is considered to be one of the indices to be used for building structural health monitoring in the future.

The measurement records used in this paper so far have only received earthquakes with a seismic intensity of about 4, and the displacement amplitude and strain amplitude are small. Moreover, the measurement location is also limited, and sufficient quantitative analysis has not been achieved. By increasing the number of measurement points and continuing measurement, and by observing the transition of the stress sharing of column beams and non-structural materials in the event of a larger earthquake, by elucidating the resistance mechanism not only in large earthquakes but also in small and medium earthquakes It is expected to advance data acquisition for more rational structural calculation and structural design.

References

- [1] Iyama J, Araki K (2020): Estimate of stress distribution based on strain measurement in actual steel building, *J. Structural Engineering*, 66B, in printing, 2020.3. (In Japanese)
- [2] Araki K, Iyama J (2018) : Joint yield moment degradation caused by out-of-plane deformation between base plates of attachment and beam flange - Study of web-clamped beam-to-column connection Part 3-, *J.Strct.Constr. Eng. , AIJ*, 83(753), 1677-1687, 2018.11 (In Japanese)
- [3] Araki K, Iyama J (2019) : Field study of fabrication time for web-clamped beam-to-column connection, *AIJ J. Technol. Des.*, 25(60), 579-584, 2019.6 (In Japanese)
- [4] Araki K, Iyama J (2017) : Numerical study on shear panel behavior of panel zone in web-clamped type connection, *16th world conference on earthquake engineering*, Santiago, Chile, 2013. 1